Avalanche statistics of fluctuation-induced fluxes from the SLPM and the W7-AS stellarator

To cite this article before publication: Jose Angel Mier *et al* 2024 *Plasma Phys. Control. Fusion* in press https://doi.org/10.1088/1361-6587/ad42d2

Avalanche statistics of fluctuation-induced fluxes from the SLPM and the W7-AS stellarator

J. A. Mier*[1], J. Blanco[1], R. Sánchez[2], O. F. Castellanos[3], D. E. Newman[4], E. Anabitarte[1], and J. M. López[5]

[1]Departamento de Física Aplicada, Universidad de Cantabria, 39005 Santander, Spain
[2]Departamento de Física, Universidad Carlos III de Madrid, 28911 Leganés, Madrid, Spain
[3]Universidad Estatal Península de Santa Elena, Vía Santa Elena−La Libertad, km 1, La Libertad, Ecuador
[4]Department of Physics, University of Alaska, Fairbanks, AK 99775-5920, USA
[5]Instituto de Física de Cantabria (IFCA), CSIC−Universidad de Cantabria, E-39005 Santander, Spain

Abstract

Measurements of fluctuating floating potentials and ion saturation currents at different radial locations in the Santander Linear Plasma Machine [Castellanos *et al.*, Plasma Phys. Control. Fusion **47**, 2067 (2005)] and at the edge of the W7-AS stellarator by means of radially movable Langmuir probes allow to infer the corresponding fluctuation-induced radial flux temporal series. Avalanche-like transport events are identified in the time series and statistically characterized in terms of avalanche size/duration/quiet-time distributions and size-duration scaling relations. Transport is diffusive in the inner and intermediate radial region of the SLPM $r < r_{\rm tr} \approx 2.6$ cm, undergoing a transition at $r_{\rm tr}$, becoming non-diffusive in the outermost region of the device, $r > r_{\rm tr}$. The results obtained at the edge of the W7-AS stellarator are similar to those found in SLPM for $r > r_{\rm tr}$, i.e., consistent with what would be expected for scale-free, self-similar plasma transport dynamics near a critical state.

I. Introduction

The subject of anomalous transport in fusion plasmas has been extensively studied in order to control and enhance the quality of particle and energy confinement in the corresponding fusion devices. After more than 50 years, the nature of this kind of transport remains still not fully understood and is an area of active research. First, a purely diffusive model was proposed leading to gyro-Bohm scaling[1], but later studies and commonplace experimental observations confirmed that transport coefficients can vary in a mixed way between gyro-Bohm and Bohm scaling[2, 3]. Most of these studies were performed in confining devices such as tokamaks and stellarators where hot, fully-ionized plasmas are generated, and experimental evidence points to intermittency in the form of avalanches or bursts of activity as an explanation for the transport dynamics[4, 5, 6]. Since temperatures in the core of these plasmas are typically of the order of several keVs, there is an inherent impossibility in performing experimental measurements in their innermost regions with some measuring device made of any material.

The experimental determination of fluctuation-induced radial fluxes has been traditionally carried out by means of Langmuir probes, so measurements at the edge plasma column of these devices are the only allowed. Apart from Langmuir probes, the heavy ion beam probe diagnostic allows studies of particle fluxes in core plasmas at tokamaks[7, 8] and stellarators[9]. Characteristic plasma radial locations such as the separatrix (boundary between closed and open field lines), last closed magnetic surface (LCMS), the shear layer (reversal in the phase velocity of fluctuations), etc, determine natural points of reference for these studies, providing convenient ways to compare the features of fluctuating quantities in different magnetic confinement devices. The general conclusions may exhibit in certain regimes non-diffusive features such as long-term memory, non-local transport or self-similarity in the dynamical space-time domain known as mesoscale. Conversely, analogous studies for plasmas generated in linear or purely toroidal (rotational-transform-less) devices show different results, usually of a more diffusive-like nature[10, 11, 12, 13]. The diffusive character of transport dynamics found in these devices must be classified in the same category as that found in previous works in the context of diffusive sandpiles[14, 15, 16] or in numerical simulations of drift-wave turbulence in fusion plasmas[17, 18]. In those processes, a coexistence and interplay takes place between (at least) two different transport channels, one of them being diffusive (that can be due to various sources such as classical and neoclassical channels or supercritical turbulence, for instance), always active, the other being inherently intermittent in nature and associated to near-marginal turbulence. The basic dynamics usually present a strong dependence on the strength of the subdominant diffusive transport channel relative to the avalanche-like, transport channel.

In this work, we focus instead on the identification and characterization of flux burst events, or avalanches, in a linear plasma inside a non-confining device (SLPM[19, 13]) and in a toroidal plasma inside a confining device (W7-AS stellarator[20, 21]). Fluxes are obtained by means of Langmuir probes inserted in the plasma. Single avalanches are then identified by choosing an appropriate threshold. Then, the statistical properties of avalanche-like events derived from the flux time series are analyzed: avalanche sizes, avalanche durations and inter-avalanche quiet times. Avalanching processes in real plasmas have been postulated as a possible explanation for the observation of non-diffusive propagation (i.e., superdiffusion) and the physical picture goes as follows, assuming the profiles are marginally stable (i.e., very close to unstable): any small perturbation can trigger an avalanching process in which nearby locations are successively destabilized, thus propagating the initial perturbation very quickly (at least, much faster than simple diffusion). Whenever these con-

*E-mail address: joseangel.mier@unican.es

ditions hold, transport dynamics should be expected to lack any characteristic length or time scale, since the radial extent of any avalanche is only limited by the size of the device. Furthermore, after the event of an avalanche, the profiles suffer the corresponding erosion, which would condition future transport events, providing the system a way to store long-term memory, at least for time scales much longer than the turbulence decorrelation time.

The results found for the dynamics of transport in SLPM, when studied from the perspective of event burst sampling, point, in general, to a rather diffusive behaviour for timescales well above the turbulence decorrelation time, except at the outermost radial locations in the plasma column (see below). The dynamics in W7-AS (at the single radial location where experimental data is available), is markedly non-diffusive (i.e., long-term memory effects, non-local transport, self-similarity over a broad range in the space-time domain, etc) as stated above, consistent with previous work on this[23, 22] and other magnetically confined hot plasmas[24, 25]. The results presented in this work do not exclude the possibility of finding non-diffusive features at the central region of linear plasmas, since all results reported in this work are only valid for the operating regimes where the present measurements were performed.

The paper is organized as follows. In Sec. II., the experimental arrangements are described, and the main plasma parameters are given. The methodology for the characterization of plasma transport dynamics via avalanche-like events sampling, as well as some theoretical concepts related with complex dynamics such as self-similarity, criticality, correlations and memory effects are given in Sec. III.. Results coming from the statistical description of avalanche-like events are presented in Sec. IV. for SLPM and in Sec. V. for W7-AS. Finally, the discussion and conclusions are presented in Sec. VI..

II. Experimental arrangements and plasma parameters

We analyzed avalanche-like events at different radial locations inside the plasma column generated in the SLPM, and at the plasma edge inside the stellarator W7-AS. The data were obtained by means of Langmuir probe measurements.

A. Set up and parameters

1. SLPM

In Ref. [13], the radial electron fluxes generated by the $\mathbf{E}\times\mathbf{B}$ turbulent flow in a linear plasma machine were studied. The experimental device is schematically shown in Fig. 1(a). The plasma is produced by launching longitudinally electromagnetic waves with a frequency $f = 2.45$ GHz along the static magnetic field B_0 by means of a circular waveguide. The magnetic field is generated by a set of six coils, water cooled, concentric with the waveguide, and arranged in Helmholtz configuration to make the axial magnetic field as homogeneous as possible. Each coil has a minor radius of 125 mm, major radius of 180 mm, and width of 43 mm. In order to reduce the reflected power on the microwave generator, the glass vessel has a conical tip facing the microwave generator. The power given by the generator ($P_{\rm LMG}$) is in the range 0.6 kW $< P_{\rm LMG} <$ 6 kW, operating the whole system in a continuous regime. The source of electromagnetic oscillations is a magnetron and the power coming from the microwaves is sent to the polarizer, which is made up of a turnstile junction [26]. Therefore, we are dealing with an electromagnetic wave transformation in a longitudinally magnetized plasma waveguide (LMG plasma column).

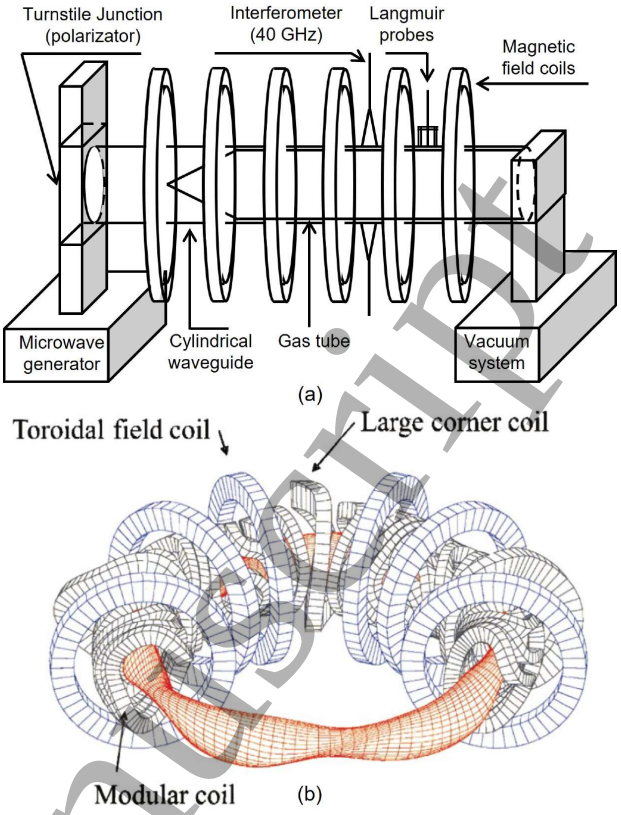

Figure 1: Scheme of (a) the SLPM and (b) the magnet system of W7-AS (Fig. taken from Ref. [22]).

The plasma is placed in a cylindrical glass vessel[19] with an internal diameter of 7 centimeters and 100 cm length (see Fig. 1), which in turn is located inside a circular waveguide 8 centimeters in diameter.

All measurements were performed for Helium plasmas with a magnetic field $B = 0.12$ T. The base pressure in the vacuum chamber is in the 10^{-6} torr range. The mean electron density is determined by using a 40 GHz interferometer. An array of Langmuir probes provides the local value of the electron density and floating potential, as well as their fluctuations across the whole plasma radial column. Table 1 shows typical plasma parameters.

Table 1: Typical plasma parameters and operating conditions in SLPM and W7-AS.

Parameter	SLPM	W7-AS
Major radius (R_0)	∞	2 m
Minor radius (a)	0.03 m	0.13−0.18 m
Magnetic field (B_0)	0.12 T	1.25−2.5 T
Electron temperature (T_e)	$\sim$ 20 eV	$\sim$ 1 keV
Electron density (n_e)	$\sim 10^{17}$ m^{-3}	$\sim 10^{19}$ m^{-3}
Ion temperature (T_i)	$\sim$ 0.05 eV	$\sim$ 1.5 keV
No. toroidal/axial coils	6	45+10
Heating power	$\sim$ 5 kW	$\sim$ 5 MW
Plasma volume	$\sim$ 0.03 m^3	$\sim$ 1 m^3

2. W7-AS

W7-AS device was a flexible system composed of 45 modular coils producing both toroidal and poloidal field components. It is equivalent to 5 toroidally connected mirrors, each one composed

of 2 planar and 9 non-planar coils[22]. The schematic of the coil system for this device is illustrated in Fig. 1(b) and table 1 shows typical plasma parameters.

In the case of W7-AS, data comes from a reciprocating Langmuir probe, with different pins distributed in the poloidal direction, half of them used to measure the ion saturation current fluctuations and the other half to measure the floating potential fluctuations. Since it is a reciprocating probe, it moves from the scrape-off layer towards the inner region of the plasma, covering a distance of about 6 cm. All the details of the experiment can be found in Ref. [27]. The data set corresponding to discharge 35427 was studied. Heating in that discharge was provided by 200 kW of ECRH, leading to a larger electron temperature, $T_e \sim 1$ KeV, than ion temperature, $T_i \sim 0.4$ KeV. The line integrated density was $\bar{n}_e \sim 3 \times 10^{19}$ m^{-3} and the magnetic field was $B_0 \sim 2.5$ T. The sampling rate for data acquisition was 0.5 MHz, and the total number of data points per pin 800000. Since we are interested in a fixed radial position, the subset corresponding to temporal entries between 350001 and 550000 has been selected (i.e., 200000 usable points equivalent to 100 miliseconds), since for longer input the probe can no longer be considered as stationary. The decorrelation time of the fluctuations is, for this case, of the order of several microseconds. Thus, we can analyze the behavior in both the fluctuation range, $t \lesssim 10$ μs, and the mesoscale range $t \gg 10$ μs.

B. Langmuir probes

The set of Langmuir probes consists of four tips of tungsten wire (each of 0.5 mm in diameter and 2 mm long) working on triple probe configuration since they are arranged in a square array of a lateral length of 2 mm (see Fig. 2), allowing the estimation of : 1) ion saturation current, I_s, and 2) floating potential, ϕ_f along the whole plasma radial column. One of the probes is in the ion saturation regime, while two poloidally separated probes remain unbiased in order to measure the floating potential. Therefore, radial fluxes can be derived from the measures of I_s and ϕ_f. The location of the Langmuir probes inside the plasma column can be fixed during the discharge, being radially modified for different discharges (SLPM) or can move radially during the discharge (W7-AS), enabling to analyse possible changes of plasma transport properties depending on radial location. Any measure can be digitized at $f_s^{\text{SLPM}} = 1$ MHz sampling frequency (SLPM), $f_s^{\text{W7-AS}} = 0.5$ MHz sampling frequency (W7-AS). Time series last 200 miliseconds for SLPM data and 100 miliseconds for W7-AS data. Therefore, temporal records are comprised of 2×10^5 points for both. Fluctuating quantities are indicated by a tilde and are constructed by subtracting the temporal average from the measured magnitude. Therefore, fluctuations are defined as having zero time-averaged value. The tip on the ion saturation regime is biased at a fixed voltage to estimate electron density fluctuations. The Langmuir probe measures the ion saturation current, $I_s \propto n\sqrt{T_e}$, which is not the same as the electron density. Therefore, fluxes inferred from these measurements are not strictly equal to the particle flux, but measurements of temperature fluctuations at the plasma edge in different confinement devices such as the TEXT and TJ-I tokamaks, show that their relative phase is such that radial particle fluxes calculated from ion saturation current and floating potential is a good estimate of local particle fluxes[28, 29].

The $\mathbf{E} \times \mathbf{B}$ fluctuation-induced radial particle flux is computed as $\Gamma = \tilde{n}\tilde{V}_r = \tilde{n}\tilde{E}_\theta / B = \tilde{n}(\tilde{\phi}_2 - \tilde{\phi}_1)/(r\varepsilon B)$, where $\vec{V}_r$ is the $\mathbf{E} \times \mathbf{B}$ drift velocity of a charged particle in the presence of an electromagnetic field. The density fluctuations, $\tilde{n}(r,\theta,t)$, are estimated through the measured values of the ion saturation current, $I_s \propto n\sqrt{T_e}$. Fluctuating poloidal electric fields, $\tilde{E}_\theta$, are estimated through the measured values of the electrostatic potential plasma fluctuations at two nearby positions, $\tilde{\phi}_1(r,\theta,t)$ and $\tilde{\phi}_2(r,\theta+\varepsilon,t)$, poloidally displaced ε radians. Here, θ is the poloidal position of the tip on the ion saturation regime, r is the radial position where the Langmuir probes are located, ε is the poloidal displacement between the two poloidally separated probes on the floating potential regime. Finally, B_0 is the axial magnetic field.

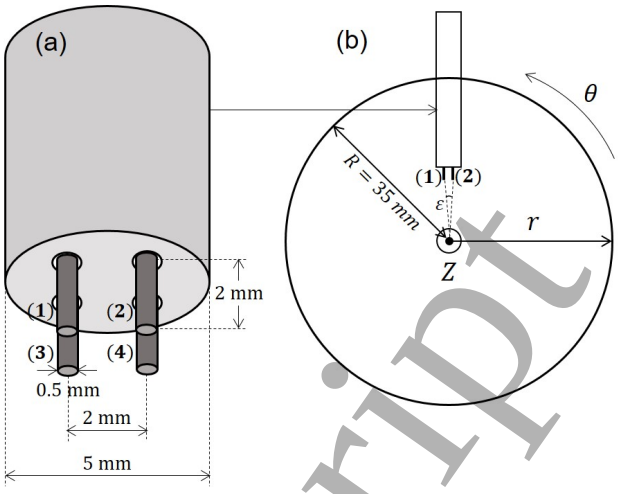

Figure 2: (a) Array of Langmuir probes and (b) plasma cross section and arrangement of Langmuir probes in the upper part of the SLPM.

III. Characterization of transport dynamics via avalanche-like events sampling

Many works in the field of plasma turbulence are devoted to the study of time series looking at them as single random processes. Then, different features are discussed such as self-similarity and memory, in trying to characterize the underlying transport dynamics, but alternative approaches to look for evidences of complex/non-trivial (diffusive/trivial) dynamics exists. Focusing, for instance, on the instantaneous flux time series derived from the measures by means of Langmuir probes, one realizes that it fluctuates rapidly in time, due to intrinsic background gaussian fluctuations in the short time-scale. Furthermore, the same would happen if we could arrange a multi-point measurement setup from which instantaneous flux fluctuations could be visualized as a function of the radial position: spatial fluctuations would be apparent due to intrinsic background gaussian fluctuations in the small space-scale. But in addition to these apparently uncorrelated fluctuations, significant transport events (i.e., "avalanches") are sometimes triggered in order to relax any instability generated in the plasma. If one of these big events passes by the probe position, the corresponding measured flux will be significantly larger than the mean over the lapse of time the avalanche is passing, typically much longer than fluctuation time scales. A commonly used technique to detect these passings is the amplitude thresholding that filters out the small gaussian fluctuations and allows to identify these transport events easily. Methods to choose the threshold commonly found in the literature[30, 23, 31] are to consider that an event is passing whenever the intensity gets larger than, say, 1) a small percentage (e.g., 10%) of the maximum, 2) a few times the mean of the absolute value of the signal, 3) a few times the standard deviation of the signal, etc. In fact, we checked

that, for all the calculations in this work, results are quite insensitive independently of the method, as long as the value of the threshold is high enough.

The aim of our analysis is to quantify the statistics of distinct properties of avalanche-like events associated to turbulence such as their size, their duration and their inter-avalanche quiet times. Figure 3(a) shows the time trace of the fluctuating $\mathbf{E}\times\mathbf{B}$ radial

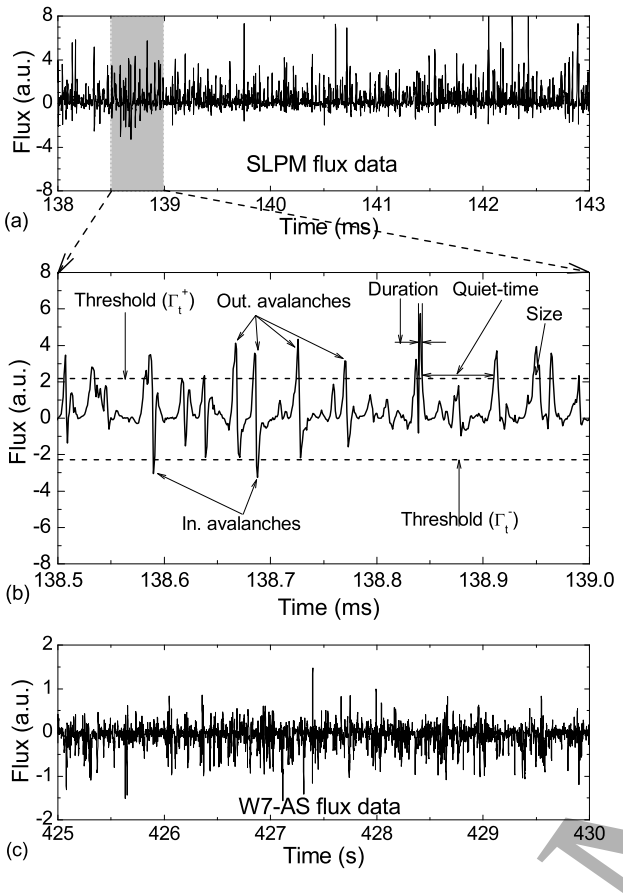

Figure 3: (a) Time trace of raw SLPM flux at r = 2.0 cm. (b) Same trace as in (a), but only during a 0.5 milisecond interval [shaded region in (a)], to better appreciate the details. Dashed lines stand for amplitude thresholds. Relevant definitions associated with avalanches are sketched. In (c), a time trace of raw W7-AS flux is plotted.

flux at $r = 2.0$ cm measured in SLPM for a lapse of time of 5 miliseconds. For each radial position, the complete series lasts for 0.2 seconds (i.e., 200000 entries). In Fig. 3(b), the same signal is zoomed in a time window of 0.5 miliseconds to better show the abrupt fluctuations of the flux around the background. In previous work[23], the signal used to be smoothed in order to eliminate local faster fluctuations, mixed with avalanches crossing the probe location. The signal was convoluted with m-point smoothing windows, before being analyzed. However, in this work the original signal is studied without smoothing (i.e., $m = 0$), since smoothing does not greatly affect the results. Avalanches can be considered, in general, as the evolution (in time and space) of an initial perturbation followed by successive relaxations that eventually cross the probe location. Thus, avalanche-like events should be longer in time than local fluctuations. An illustration of the main concepts related to avalanches are depicted in Fig. 3(b). The "duration" of an event can be defined as the lapse of time during which the signal remains above (below) the positive, Γ_t^+, (negative, Γ_t^-) threshold. The "size" of an event is defined as the area enclosed between the signal and the threshold during that lapse of time. The inter-avalanche "quiet-time" can be defined as the period of time between two consecutive events. At this point it is important to mention that avalanches are defined both outwards (positive bursts) and inwards (negative bursts). By inspecting Fig. 3(b), it turns out that durations, sizes and quiet-times depend on i) the amplitude threshold and ii) the number of points in the smoothing (not performed in this work). Finally, in Fig. 3(c), a fraction of the electrostatic turbulent flux data measured in W7-AS is shown for a time lapse of 5 miliseconds for comparison purposes.

A. Event size and duration: Self-similarity and criticality

Assuming that transport is dominated by avalanching processes, different conclusions can be drawn from the analysis of the statistics of the relevant quantities characterizing the transport events such as avalanche durations and avalanche sizes. Self-similar (or scale-invariant) dynamics require that the avalanching process dominating transport lacks any characteristic scale. In such a case, the statistics of the corresponding quantities exhibit power law behaviour since mathematical functions remain invariant[32] for certain rescaling factors of the independent variable. The mathematical archetype of scale-invariance is the power law function, $f(x) = x^{\alpha}$, for any real α.

Furthermore, self-similar critical dynamics require that the avalanching processes taking place in our system (and generating particle transport) lack any characteristic scale, being only limited by the system size. This translates into the divergence of the first-order moment of the distribution, the mean, associated to any positive definite quantity such as avalanche sizes or avalanche durations. For instance, the probability density function (pdf) of both, sizes (S) and durations (T) scale respectively as,

$$p(S) \sim S^{-(1+b_S)}, \quad 0 < b_S < 1 \tag{1a}$$

$$p(T) \sim T^{-(1+b_T)}, \quad 0 < b_T < 1 \tag{1b}$$

leading to the following mean sizes and durations,

$$\langle S \rangle = \int_0^{S_{\max}} \mathrm{d}S \cdot S \cdot p(S) \propto S_{\max}^{1-b_S}, \tag{2a}$$

$$\langle T \rangle = \int_0^{T_{\max}} \mathrm{d}T \cdot T \cdot p(T) \propto T_{\max}^{1-b_T}, \tag{2b}$$

that diverge respectively with the limits imposed by the system size, $S_{\max}$, and system duration, $T_{\max}$.

B. Inter-events quiet-times: Correlations and memory

Avalanche triggerings are, in general, not random but dictated by memory manifested in the long-range temporal scale (i.e., temporal scales much longer than the temporal decorrelation of the turbulence). The way complex systems such as fusion plasmas can store memory is, for instance, through the shape of their profiles which, by the way, remain rather insensitive to the effects of the external drive[33]. Avalanches tend to be triggered around those locations that are closest to some instability threshold since they are the most likely to become unstable under the perturbation of the external drive. In the same logic, avalanches will tend to stop around those locations where the profiles are far enough from that threshold, since now they cannot propagate further even after the relaxation at neighbouring locations. Thus, the pdfs of both avalanche triggering and stopping locations are strongly influenced by the previous history of the system[34], being the mechanism responsible for the implementation of memory in the system in the long-range temporal scale.

Memory effects can be tracked from the conditional sampling analysis by studying the statistics of inter-avalanche quiet-times.

If one considers avalanches as a point process (i.e., an ordered set of events, with zero duration, that are consecutively triggered in time[35]), then, in the absence of any temporal correlation between triggerings, it becomes a Poisson process, whose quiet-time statistics should follow an exponential pdf,

$$p(Q) \sim \tau_0^{-1} \exp(-Q/\tau_0), \tag{3}$$

with τ_0 giving the average time between triggerings or average quiet-time, and τ_0^{-1} being the average triggering rate. Poisson processes lack any memory effects by definition.

When long-term, self-similar correlations between events are present, the quiet-time pdfs would exhibit asymptotic power laws given by[23],

$$p(Q) \sim Q^{-(1+\lambda)}, \quad 0 < \lambda < 1. \tag{4}$$

As for the case of avalanche sizes and durations, where the lack of spatial and temporal scales translated into the avalanches exhibiting scale-free statistics as shown in Eqs. (1a) and (1b), the distribution of quiet-times given by Eq. (4) again ensures that no mean quiet-time can be defined, except the fact that real systems are always limited both in size and time.

IV. Statistics of avalanche-like events from fluctuation-induced radial fluxes in SLPM

In this section we report the results of an analysis of flux fluctuations that aims at identifying avalanche-like processes in the plasmas generated in the SLPM. The analysis was performed by considering the statistics of distinct properties based on avalanche-like events associated to turbulence such as avalanche sizes/durations and quiet-times between avalanches.

As shown in the previous section, the number of experimental entries for the fluctuation-induced flux series is scarce and not enough in order to construct well-defined avalanche size and avalanche duration probability density functions. Therefore, survival functions (sf) have been used instead of the more common pdfs. The survival function is also known as complementary cumulative distribution function[36],

$$p_>(x) \equiv \overline{F}_X(x) \equiv 1 - F_X(x) \equiv P(x > X), \tag{5}$$

since it complements the information of the cumulative distribution function, $F_X(x) \equiv P(x \leq X)$. From now on, we will reserve $p_>(x)$ for the survival function. The survival function is often used in health sciences since it gives the probability of an individual surviving beyond time x. It is a non-increasing function with the following properties: $p_>(0) = 1$ and $p_>(\infty) = 0$. The survival function is the integral of the probability density function,

$$p_>(x) = \int_x^\infty p_X(x)dx \implies p_X(x) = -\frac{dp_>(x)}{dx}. \tag{6}$$

For specific cases were $p_X(x)$ exhibit exponential or power law behavior, the corresponding survival function will behave in the same way.

Local fluctuations are separated from avalanches by amplitude thresholding as shown in Fig. 3(b). Avalanches are defined as bursts or activity exceeding the corresponding threshold. Different thresholding methods have been described in the literature to do this separation of events[37, 30]. Alternative methods to identify avalanches without thresholding have also been described[38] for cases where the signal is weak and/or the ratio between the signal and the noise is low. In such cases, making use of thresholds is inappropriate. Our measurements allow the use of thresholds since the amplitude associated to local bursts is, in general, quite large when compared to background level (i.e., signal to noise ratio is reasonably high, see Fig. 3). In our calculations we used different levels and found that setting upper (Γ_t^+) and lower (Γ_t^-) thresholds at a specific percentage of the mean first $n = 10$ maxima, $\{\Gamma_i^{\max},\ i = 1,\ldots,n\}$, and minima, $\{\Gamma_i^{\min},\ i = 1,\ldots,n\}$ of the series, i.e., $\Gamma_t^+ = (\sum_{i=1}^{i=10} \Gamma_i^{\max})/n$ and $\Gamma_t^- = (\sum_{i=1}^{i=10} \Gamma_i^{\min})/n$, is a good choice. There is a correspondence between choosing some percentage of the mean first n positive-maxima/negative-minima and choosing some other percentage of standard deviation of data. This thresholds should be as high as possible in order to separate better real avalanches from local faster events, but setting arbitrarily high threshold values leads to an unacceptable worsening of statistics.

As stated above, in order to find out whether pdf tails follow exponential or power law behaviour (and to obtain the corresponding exponents), it is not needed to construct the pdf. This information can be obtained by means of the survival function. One just wants to know whether the pdf has an exponential/power law tail and to estimate its exponent. The scaling of exponential, $p_1(x)$, or power law, $p_2(x)$, probability density functions entails identical scalings for the corresponding survival functions, $p_{>_1}(x)$ and $p_{>_2}(x)$:

$$p_1(x) \sim \exp(-x/x_c) \Longrightarrow p_{>_1}(x) \sim \exp(-x/x_c), \tag{7a}$$

$$p_2(x) \sim x^{-(1+\alpha)} \Longrightarrow p_{>_2}(x) \sim x^{-\alpha}, \tag{7b}$$

given the definitions in Eq. (6). Hence, if $p(x)$ exhibits exponential/power law behaviour at some x-interval, so does the corresponding survival function $p_>(x)$.

For a given avalanche, we calculate its size S (the integral of the positive/negative flux over the avalanche duration or area enclosed between the positive/negative flux and the reference given by the positive/negative threshold), and its duration T (time lapse during which the positive/negative flux remains above/below the positive/negative threshold). Finally, for two consecutive avalanches (regardless of whether they are outwards or inwards), the time lapse between the end of the first one and the beginning of the next one, or quiet-time Q, is also computed.

A. General avalanche statistics

As seen previously in the definition of an avalanche, Fig. 3, a proper choice of the amplitude threshold is crucial in order to obtain reliable results. On the one hand, an arbitrarily small value for this parameter leads to the inclusion of non-avalanche events as avalanches. Conversely, an excessively large value for the threshold results in too few avalanches, making it challenging to gather the necessary statistics to draw any conclusions about transport dynamics. Since this is a fundamental parameter that will significantly impact the subsequent results, it is essential to conduct a preliminary study on its influence on the basic statistics of avalanches. Figure 4(a) shows the dependency of the number of avalanches as a function of the amplitude threshold value at different radii. It is worth remembering that the threshold has been set in terms of a percentage relative to the maximum/minimum of the temporal records. In turn, the maximum/minimum have been calculated as the average of the 10 highest/lowest values of the series. For arbitrarily low values of that percentage, the amount of avalanches tends to be half of the total amount of entries (i.e., 10^5 for SLPM data). As the threshold parameter increases, the

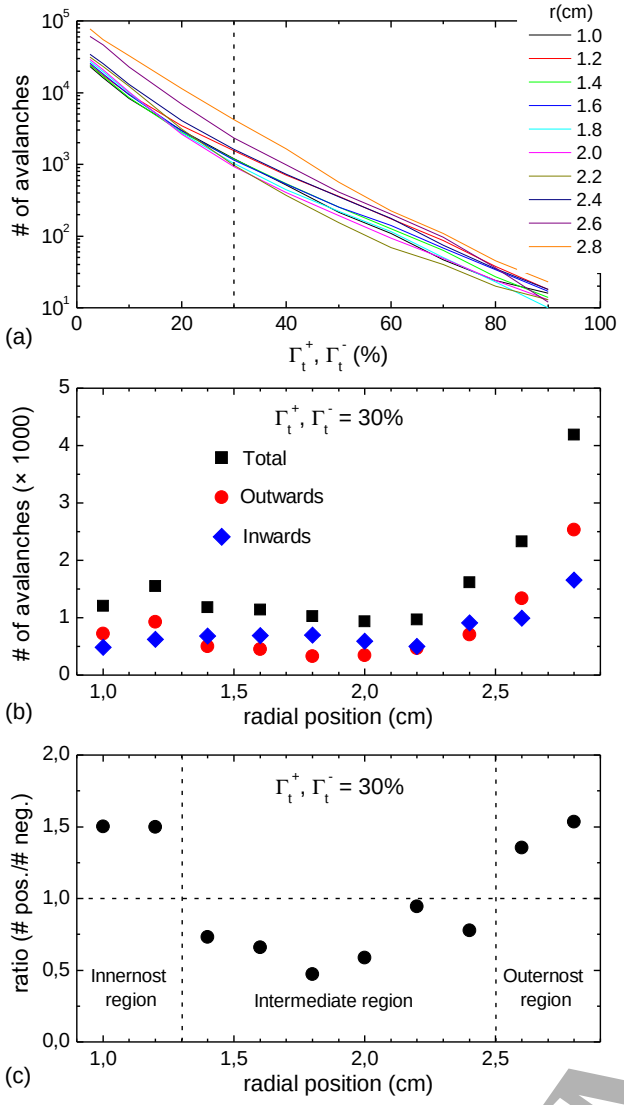

Figure 4: (a) Total amount of avalanches vs. amplitude threshold at different radii. (b) Radial dependence of the number of avalanches for a given threshold. (c) Radial dependence of the ratio between positive and negative avalanches for a given threshold. The parameters used to calculate avalanche statistics are $\Gamma_t^+ = \Gamma_t^- = 0.3$.

amount of avalanches smoothly decrease, tending to zero for percentages approaching 100%. The dashed, vertical line in Fig. 4(a) represents the value for the percentage used in this work (i.e., 30% of the maximum). This value allows to gather amounts of avalanches in the range $\sim (1000 - 4000)$ depending on radius, which is enough to draw the corresponding survival functions. In Fig. 4(b), the radial dependence of the total/positive/negative number of avalanches is shown. Positive/negative avalanches are defined as transport events radially outwards/inwards. At the innermost and outermost regions of the plasma (i.e., $r < 1.3$ cm and $r > 2.5$ cm), positive avalanches outnumber negative ones. In contrast, at intermediate radii (1.3 cm $< r <$ 2.5 cm) the opposite is true, even though the net electron flux is always positive. In Fig. 4(c), the ratio between positive and negative avalanches is represented. The dashed horizontal line represents the balance between positive and negative avalanches. The dashed vertical lines located at $r = 1.3$ cm and $r = 2.5$ cm represent the frontiers between the innermost/intermediate and intermediate/outermost regions of the plasma column.

From now on, different variables and labels will be used to denote the value of the avalanche exponents and characteristic quantities estimated in this work. Table 2 shows their names and expressions/symbols.

Table 2: Nomenclature of the avalanche mean-field exponents and key variables.

Name	**Expression/symbol**
Size exponent: γ_S	$p_>(S) \sim S^{-\gamma_S}$
Duration exponent: γ_T	$p_>(T) \sim T^{-\gamma_T}$
Quiet-time exponent: γ_Q	$p_>(Q) \sim Q^{-\gamma_Q}$
Typical average size: S_c	$p_>(S) \sim \exp(-S/S_c)$
Typical average duration: T_c	$p_>(T) \sim \exp(-T/T_c)$
Typical average quiet-time: Q_c	$p_>(Q) \sim \exp(-Q/Q_c)$
Size-duration exponent: γ_{ST}	$\langle S \rangle(T) \sim T^{\gamma_{ST}}$
Crossover duration: T_*	T_*

B. Statistics of avalanche sizes

The survival function of avalanche sizes are plotted in Fig. 5(a) at different radial positions in SLPM. No clear trend is observed for the inner radial locations ($r < 2.6$ cm), but avalanche sizes sfs seem to be exponentially distributed, $p_>(S) \sim \exp(-S/S_c)$, $S_c \simeq$ 23 a.u., for sizes above $S = 20$ a.u. For smaller sizes, no defined scaling is found and the distribution of sizes is mainly dominated by the cut-off. It is worth stressing that for $r \geq 2.6$ cm, the tails of avalanche sizes distributions present power law-like behaviour, $p_>(S) \sim S^{-\gamma_S}$, with $\gamma_S \simeq 3.0$ at the outermost radial location. This is a first indication that transport dynamics in this linear machine is changing from classical to a more complex response as we move radially outwards.

Indeed, the amplitude threshold for the determination of avalanches depends on radius since the maximum/minimum values of flux series also varies radially. The criteria followed in this work for the determination of the threshold is 30% of the maximum/minimum of the series (considering both outward and inward avalanches). This percentage is around 2 to 4 times the standard deviation of the signal, depending on the radial location. Figure 5(b) depicts the root-mean-squared value of fluctuation-induced $\mathbf{E} \times \mathbf{B}$ radial fluxes at different radial locations, showing a decreasing trend. As the averaged flux decrease with increasing radius, it turns out that avalanche sizes become smaller for the outermost radius, as shown in Fig. 5(a). A correlation is found between the decrease in avalanche sizes and the change of the local electron temperature: in the two outermost radial locations, $r = 2.6$ cm and $r = 2.8$ cm, a sharp temperature gradient is found (see Fig. 3 in Ref. [19]), while at the inner radii, $r < 2.6$ cm, the temperature profile is quite uniform, being avalanche sizes quite similar. The ratio of the avalanche-like flux to the total flux is calculated in the following way:

$$\frac{\Gamma_{\rm av}}{\Gamma_{\rm tot}} = \frac{\int_{t_{\rm ini}}^{t_{\rm end}} |\Gamma(t)| H\left(|\Gamma(t)| - \Gamma_t\right) dt}{\int_{t_{\rm ini}}^{t_{\rm end}} |\Gamma(t)| dt}, \qquad (8)$$

where $t_{\rm ini}$ and $t_{\rm end}$ are the initial and final times for data acquisition, $H(x)$ is the Heaviside step function and Γ_t is the upper threshold for the determination of avalanche fluxes. Results in SLPM are depicted in Figure 5(c) for all the radial locations analyzed. On the one hand, there is a clear dependence on amplitude threshold: the contribution of avalanche-like flux relative to the total flux increases/decreases with decreasing/increasing amplitude threshold parameter, Γ_t. On the other hand, no clear/defined radial pattern is

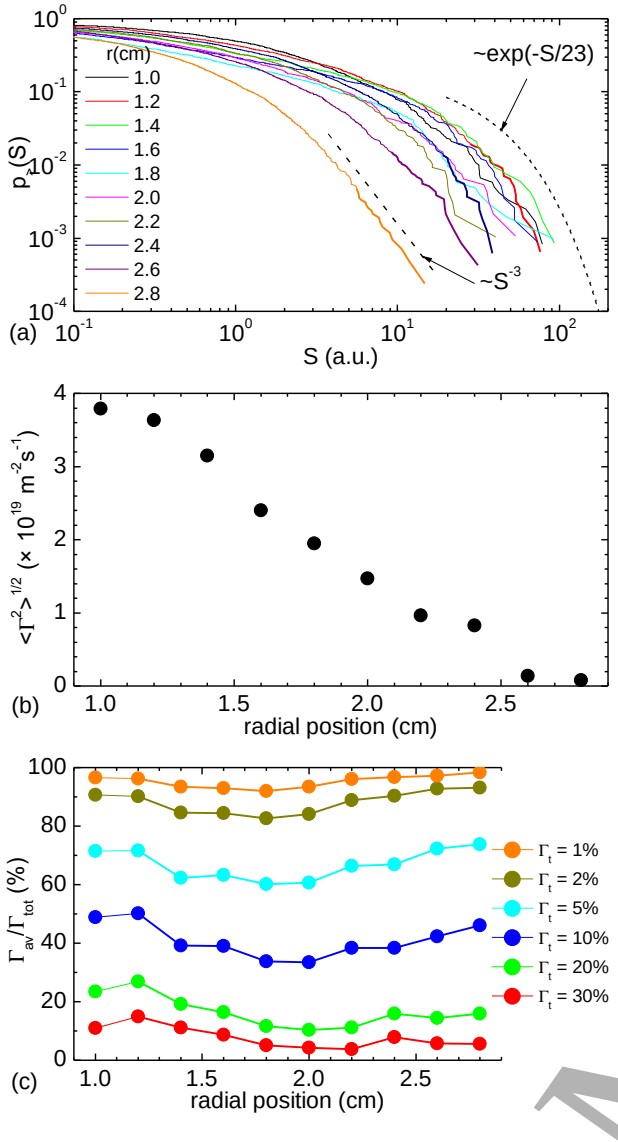

Figure 5: (a) Avalanche size survival functions at different radial locations (see legend). For comparison, exponential and power law functions are also plotted (dashed lines). The parameters used to calculate avalanche statistics are $\Gamma_t^+ = \Gamma_t^- = 0.3$. (b) Root-mean-squared values of the fluctuating $\mathbf{E}\times\mathbf{B}$ flux in SLPM. (c) Ratio of avalanche transport to total transport, Γ_{av}/Γ_{tot} (defined in the text), for different values of the amplitude threshold (see legend).

found, remaining the quotient given by Eq. (8) fairly constant for all the radii.

C. Statistics of avalanche durations

The sfs of avalanche durations are plotted in Fig. 6 at different radial positions. Avalanche durations are exponentially distributed, i.e., $p_>(T) \sim \exp(-T/T_c)$, with a typical average time $T_c = 1-3$ μs, for all locations that meet the condition $r < 2.6$ cm. This behaviour is observed for durations ranging from ~ 1 to ~ 20 microseconds. The exponential function in Fig. 6 provides a nice fit for the whole range of durations. However, at the outermost radial location ($r = 2.8$ cm), the tail of avalanche durations distribution is better described by power law decay, $p_>(T) \sim T^{-\gamma_T}$, with $\gamma_T \simeq 3.6$. This constitutes a second indication, in addition to the previous one for avalanche sizes distribution, suggesting a transient in transport dynamics in the outermost plasma region.

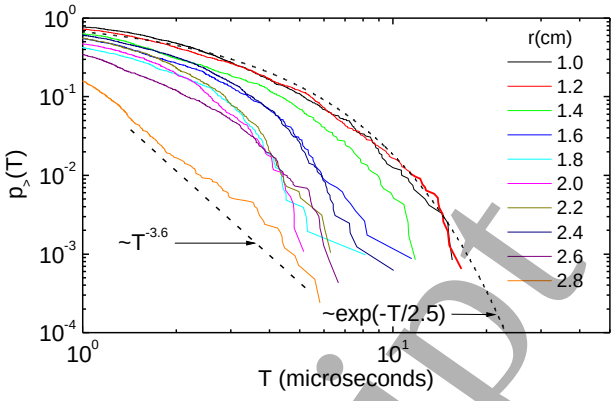

Figure 6: Avalanche duration survival functions at different radial locations (see legend). For comparison, exponential and power law functions are also plotted (dashed lines). The parameters used to calculate avalanche statistics are $\Gamma_t^+ = \Gamma_t^- = 0.3$.

D. Statistics of inter-avalanche quiet-times

Another interesting tool regarding avalanches is the statistics of the quiescent temporal lapses between consecutive bursts or quiet-times (see Fig. 2). The sfs of inter-avalanche quiet-times are plotted in Fig. 7(a) at different radial positions. For the innermost radii, $r < 2.6$ cm, quiet-times are exponentially distributed, with typical average quiet-times in the range $Q_c = 110-240$ μs, consistent with a Poisson statistics and a radial transport in a diffusive regime. The dashed exponential functions in Fig. 7(a) again provides an excellent fit for the whole range of durations. For $r = 2.6$ cm, the distribution seems to be halfway between exponential and a power law. Finally, at $r = 2.8$ cm, the distribution is perfectly described by a power law decay, $p_>(Q) \sim Q^{-\gamma_Q}$, with $\gamma_Q \simeq 0.75$, in the range $Q \sim (20-400)$ μs. This provides a third indication of a transient in transport dynamics at the two outermost radial locations: as one moves outwards from the center, the mechanisms contributing to avalanche initializations (avalanche triggerings) become correlated, manifested in the presence of power law tails in quiet-time sfs.

The shape of the distributions change with amplitude threshold values. For arbitrarily low values, all distributions are rather exponential and not clear power-law trends con be glimpsed for at least one temporal decade, as shown in Fig. 7(b) (blue line). This is independent of the underlying transport dynamics. If $\Gamma_t^+ \simeq \Gamma_t^- \ll \langle\Gamma\rangle$, non-avalanching events will be considered as real avalanches (due to the low amplitude threshold value), and self-similar traces associated to real avalanches will be masked under the gaussian background noise generated by low-intensity events.

As an example, quiet-time sfs can also be calculated by only considering avalanches exceeding a minimum duration, T_t, such that they are included in the self-similar temporal range. In Fig. 7(b) (red line), the inter avalanche quiet-time sf is plotted, but now considering those time lapses between avalanches whose duration is above some prescribed threshold duration (i.e., $T_t = 4$ μs), maintaining identical amplitude threshold ($\Gamma_t^+ = \Gamma_t^- = 0.05$). Clearly, both distributions are quite different, going from exponential when no duration thresholding is applied ($T_t = 0$ μs), to power-law-like tails (i.e., self-similar), when a duration threshold ($T_t = 4$ μs) is considered.

Besides duration thresholding, the usual amplitude thresholding also allows to unveil power laws from the noisy, uncorrelated background. Both methods result in a loss of statistics, which finally led us to use sfs instead of pdfs in this work. There is a

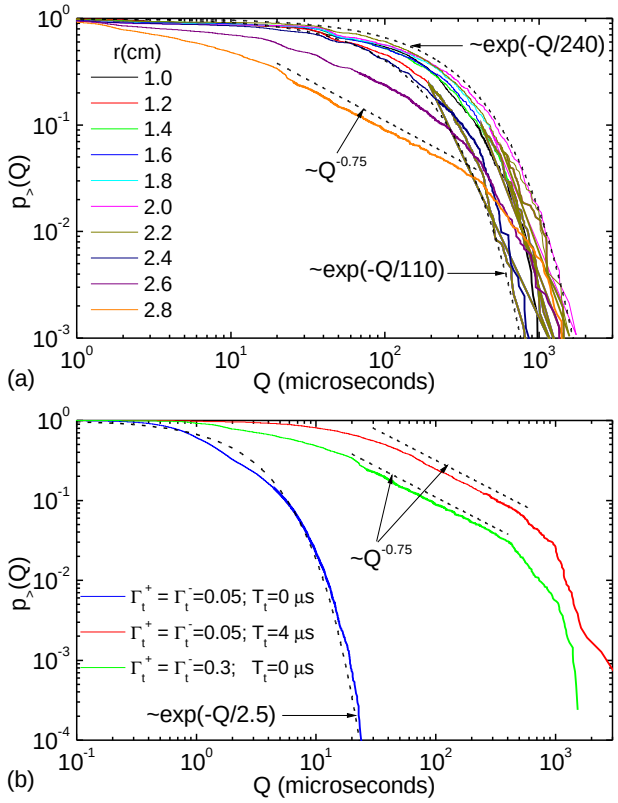

Figure 7: (a) Inter avalanche quiet-time survival functions at different radial locations (see legend). For comparison, exponential and power law functions are also plotted (dashed lines). The parameters used to calculate avalanche statistics are $\Gamma_t^+ = \Gamma_t^- = 0.3$. (b) Quiet-time survival functions at $r = 2.8$ cm using different amplitude and/or avalanche duration thresholds (see text and legend).

statistical correspondence when combining the relative intensities of the two kinds of thresholding. As an example, in Fig. 7(b) (green line) the quiet-time distribution between avalanches without duration thresholding ($T_t = 0$ μs), but with a higher value of the amplitude threshold, $\Gamma_t^+ = \Gamma_t^- = 0.3$ is shown. Despite the distributions are not identical, they maintain the same power-law trend just below the cutoff, with similar scaling exponents over the same time range.

The distribution of quiet-times between all transport events reflects the statistics of the drive [39]. If the driving mechanism is random, the pdf of quiet-times must follow a Poisson, exponential law, as shown in the previous section, Eq. (3). In our case, the driving mechanism for the triggering of bursts or avalanches is given by the fluctuations in floating potentials and ion saturation currents, experimentally measured with Langmuir probes. The distribution functions of these fluctuations are gaussian[13]. This could lead to the notion that avalanche triggering mechanisms giving rise to transport events are uncorrelated, and the distribution of quiet-times should be exponential, which is true at inner and intermediate radial regions in SLPM. At the outermost radial location where experimental data is available, turbulent transport dynamics appear to be governed by non-diffusive phenomena.

E. Relation between avalanche size and duration

Considering the relation between the average size of avalanches for a given duration, the intermittent response is characterized by avalanches having the following power law scaling relation between sizes and durations, $\langle S \rangle(T) \sim T^{\gamma_{ST}}$. There is experimental evidence revealing the existence of scale-invariance in the dynam-

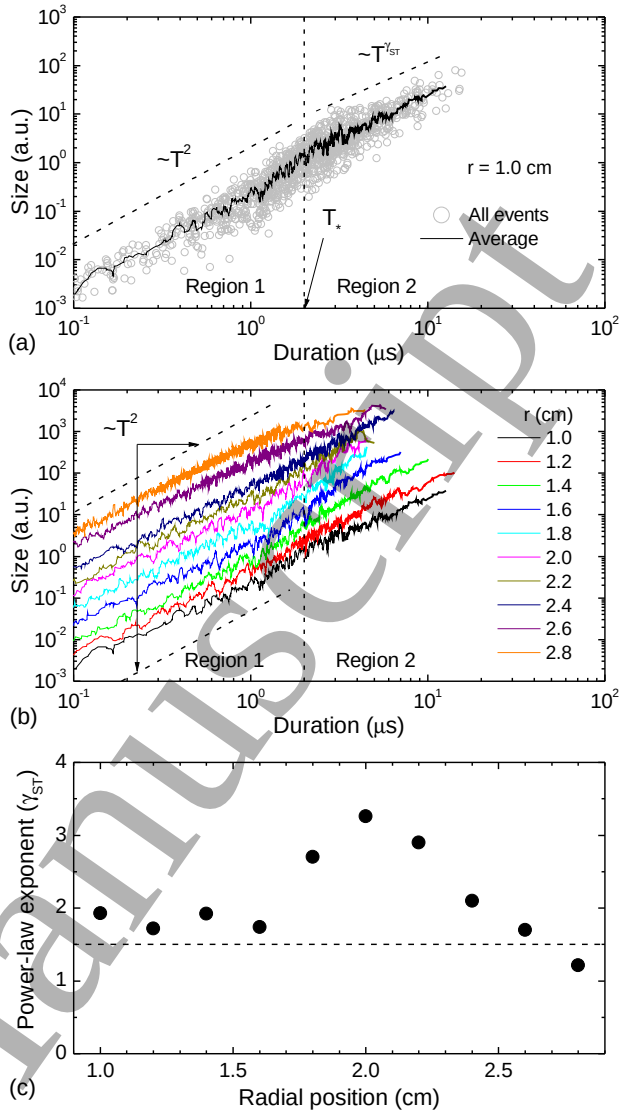

Figure 8: (a) Avalanche size versus duration for all avalanches in SLPM at $r = 1.0$ cm (light gray hollow circles) and average avalanche size for fixed duration at the same position (full black line). (b) Average avalanche size for fixed duration at different radial positions. Asymptotic power law trends, $\langle S \rangle(T) \sim T^{\gamma_{ST}}$, have been fitted for avalanche durations above the crossover duration, $T \geq 2$ μs. (c) Radial dependence of power law exponents from fits in (b).

ics of fusion plasmas[23]. In particular, the statistics of quiet-times in tokamaks and stellarators are found to be consistent with what would be expected for randomly driven systems governed by critical phenomena, i.e., Self-Organized Criticality (SOC) dynamics. It was found previously[31] that critical phenomena may only be present at the outermost radial region of SLPM from the analysis of avalanche size/duration avalanche distributions, as well as from the inter-avalanche quiet-time distributions.

Figure 8(a) depicts the size-duration relation for all avalanches at $r = 1.0$ cm (light gray hollow circles), and the average size conditioned on a given duration T, $\langle S \rangle(T)$ (full black lines). In Fig. 8(b), the average size conditioned on a given duration is plotted for all radii.

Two asymptotic scaling relations are found in region 1, $\langle S \rangle(T) \sim T^2$ for $T < T_* \approx 2$ μs, and region 2, $\langle S \rangle(T) \sim T^{\gamma_{ST}}$ for $T > T_*$. The existence of two distinct regions with crossover duration T_* is a side effect due to thresholding. For avalanche with durations below the crossover duration, $T < T_*$, all events have

a low number of values above the threshold (for instance, it may well be the case that only one point is above the threshold, thus conforming an avalanche), which is not enough to capture the internal complexity of the corresponding avalanche. In Fig. 9, an sketch of an avalanche with just three points above the threshold (dark grey, small triangle) is represented together with the avalanche size (S) and duration (T). Due to the low amount of entries, the size/duration scaling relation becomes trivially quadratic: $\langle S \rangle \sim T^2$. As an example (see light grey, big triangle in Fig. 9), when the duration is doubled ($T \to T' = 2T$), the resulting size is four times larger ($S \to S' = 4S$). Region 1 in Fig. 8(b) is associated to this quadratic scaling as a side effect of thresholding affecting the smallest avalanches. For avalanche durations longer than the crossover duration ($T \geq T_*$), the amount of experimental entries above the threshold is enough to capture the internal structure of the avalanche. The resulting exponents in our experiment are plotted in Fig. 8(c). The numerical values of the exponents at radial locations $r \leq 2.6$ cm are in the range $(1.5, 3)$, whereas at the outermost radial location its value is $\gamma_{ST} \simeq 1.2$.

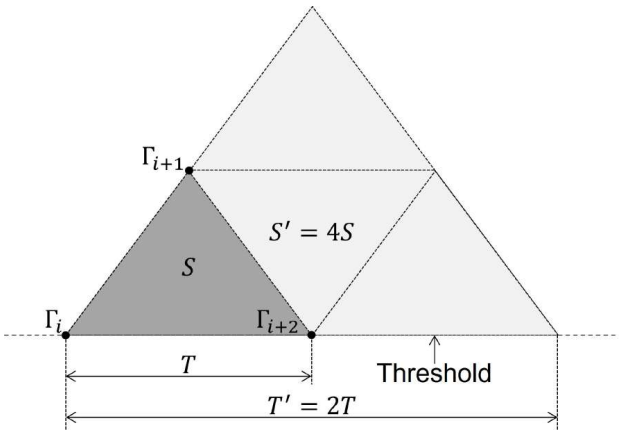

Figure 9: Scheme of the formation of an avalanche barely exceeding the threshold (dark grey, small triangle), and trivial size/duration scaling relation as a side effect of thresholding.

It is interesting to note that at $r = 2.8$ cm, the relation between exponents,

$$\gamma_{ST} = \gamma_T / \gamma_S, \tag{9}$$

seems to be satisfied, which is often found elsewhere[41, 40]. This result is quite well reproduced in this work when analyzing the radial $\mathbf{E} \times \mathbf{B}$ fluctuation-induced radial particle flux in the outer region of the plasma column. Furthermore, is consistent with those obtained for a wide range of physical processes[42, 43], suggesting perhaps that transport processes in the outer region of the SLPM could be included within the same kind of scaling universality class.

V. Results from W7-AS stellarator flux data

To compare the properties of electrostatic turbulent fluctuations in SLPM with confinement devices, a signal from the Langmuir probes in the W7-AS stellarator was also analyzed. Specifically, results from discharge 35427 were used. The signal was sampled at 2 Mega-Hertz frequency, with a total of 200000 usable points. The tips of the probe were located between 0 and 2 centimeters within the last closed magnetic surface.

Figure 10(a) shows the dependency of avalanche events (total/positive/negative) with amplitude threshold in W7-AS (identically defined as in SLPM). For low values of the amplitude threshold, the amount of avalanche events tend to be half of the total amount of entries, smoothly decreasing and tending to zero as the threshold increases. The dashed, vertical line in Fig. 10(a) represents the generic value for that threshold (in %) used in this work (the same as in SLPM). This value allows to gather 6452/3722/2730 total/positive/negative avalanches in W7-AS, which is enough to draw the corresponding survival functions.

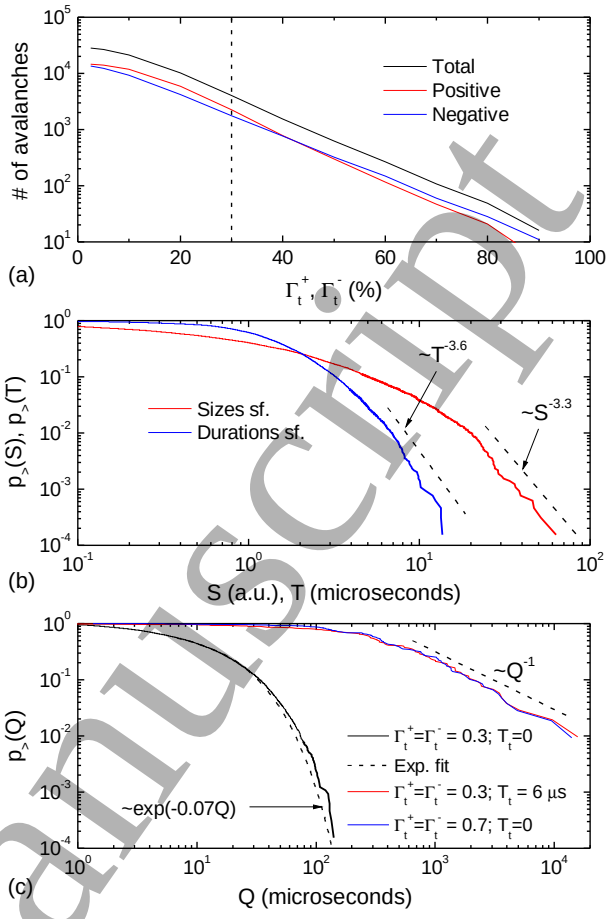

Figure 10: Results from the analysis of W7-AS electrostatic turbulent flux data for shot No. 35427. (a) Total/positive/negative amount of avalanche events. (b) Avalanche sizes/durations survival functions. (c) Inter avalanche quiet-times survival functions, with different thresholding parameters.

The distribution function of avalanche sizes is plotted in Fig. 10(b) (red line). Analyzing the shape of the sf, a power law trend becomes apparent for the highest sizes (dashed trend line), until reaching the maximum avalanche sizes in our records. It is worth noting that this result is similar to the corresponding at the outer region in SLPM, with similar decay exponent.

The distribution function of avalanche durations is plotted in Fig. 10(b) (blue line). Similar to the situation for sizes, a power law trend is glimpsed for the longest durations (dashed trend line), until reaching the maximum avalanche durations in our records ($\sim 10-15$ microseconds), just before the cutoff. Again, this result is similar to that found at the outer radius in SLPM, with similar decay exponent.

The distribution functions of the quiescent temporal lapses between consecutive bursts or quiet-times are plotted in Fig. 10(c). An exponential behaviour is obtained (see full black line) when considering quiet-times between all avalanches, regardless of their duration, i.e., $T_t = 0$ μs. The distribution can be fit well by an exponential law (dashed line), suggesting that avalanche events

crossing the position where the Langmuir probe is located, do it randomly.

We have also calculated the distribution of quiet-times for those avalanches whose duration T, are above some prescribed threshold, T_t. A different distribution is obtained in this case, [see red line in Fig. 10(c)] when only avalanches exceeding a minimum duration, T_t, are considered. We have selected avalanches lasting more that $T_t = 6$ microseconds, with identical amplitude threshold. A power law distribution is then obtained for the longest quiet-times, indicating that radial transport is taking place in a complex, non-diffusive way. By setting threshold duration values above $T_t \sim 5$ μs, inter avalanche quiet-time distribution tails become self-similar, exhibiting power-law behaviour. There is a clear correlation between the emergence of power laws in quiet-time distributions in Fig. 10(c) and the increase in T_t[23].

As in the outer radial region in SLPM, the usual amplitude thresholding allows to unmask power laws from the gaussian background, without the need of applying duration thresholding. Figure 10(c) (blue line) shows the quiet-time distribution between avalanches without duration thresholding ($T_t = 0$ μs), but with a higher value of the amplitude threshold, $\Gamma_t^+ = \Gamma_t^- = 0.7$. Virtually, both distributions [see blue and red lines in Fig. 10(c)] fall on top of each other.

It is important to emphasize that both, amplitude and duration thresholds need to be properly combined in order to capture the real dynamics. Otherwise, by non-discriminating the noisy background from real avalanches through appropriate thresholding, non-trivial features could not be detected from the signal. Depending on the specific values for Γ_t and/or T_t, different distributions are obtained.

Figure 11 shows the avalanche size-duration relation in W7-AS for all avalanches (light gray hollow circles), and the average size conditioned on a given duration T, $\langle S \rangle (T)$ (full black line). An asymptotic scaling relation is found with exponent $\gamma_{ST} \simeq 1.2$, for avalanche durations $T \geq T_* \simeq 3$ μs. The power law fit is also plotted as a red line in Fig. 11. The existence of two distinct

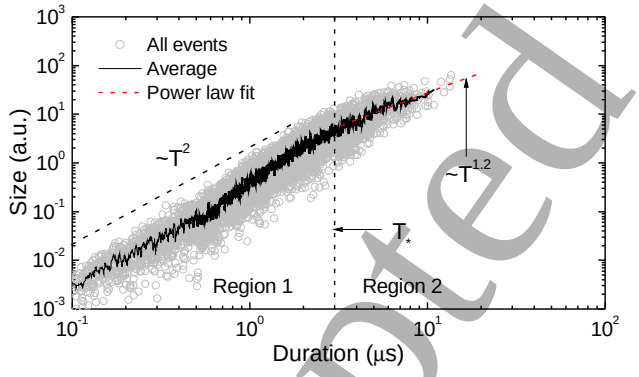

Figure 11: Avalanche size versus duration for all avalanches in W7-AS shot No. 35427 (light gray hollow circles) and average avalanche size for fixed duration (full black line). For avalanche durations in the short temporal range-scale ($T \ll T_*$), the average size scales quadratically with avalanche duration (see Fig. 9 for details). The asymptotic power law trend, $\langle S \rangle (T) \sim T^{\gamma_{ST}}$, has been fitted for avalanche durations above the crossover duration, $T \geq T_*$.

regions with different scalings in Fig. 11 (Regions 1 and 2), with crossover duration $T_* \approx 3$ μs is a side effect due to thresholding, whose explanation is exactly the same as that given previously for SLPM data in Fig. 8(b). The crossover duration in Fig. 11 is consistent with the duration in Fig. 10(b) where a power law trend is found in durations sf. In the same way, the crossover size in Fig. 11, $S_* \approx 10$ a.u. (not indicated in the plot) is consistent with the size in Fig. 10(b) where a power law trend is found in sizes sf.

Working with W7-AS fluctuation induced data, power laws are found in avalanche sizes/durations sfs, similarly to that found at the outermost radial location in SLPM. Scaling relationships are observed for avalanche sizes sfs, $p_>(S) \sim S^{-\gamma_S}$ with $\gamma_S \simeq 3.3$ over some critical size. Furthermore, scaling relations are also observed for avalanche durations sfs, $p_>(T) \sim T^{-\gamma_T}$ with $\gamma_T \simeq 3.6$ over some critical duration. Finally, an scaling relation is found in the avalanche size-duration relation, $\langle S \rangle (T) \sim T^{-\gamma_{ST}}$ with $\gamma_{ST} \simeq 1.2$. These results are consistent with Eq. (9).

VI. Discussion and conclusions

In this paper, we analyze the properties of fluctuation-induced fluxes in different radial regions of a linear helium plasma machine (SLPM), and just inside the LCMS of the W7-AS stellarator. These studies have been performed with the aim of comparing the similarities and differences in the dynamics of transport in both, cold, weakly ionized plasmas inside non-confining linear devices, and hotter, fully ionized plasmas inside confining toroidal devices. Using the same techniques employed in the past, we conclude that transport dynamics in SLPM are, in general, different from those found in the vicinity of the scrape-off-layer in confining devices such as W7-AS.

The experimental setup in SLPM allows to explore the plasma column at different radial locations in multiple discharges by means of a movable array of Langmuir probes. The measurements of the flux indicate that particle losses are intermittent and bursty, with the turbulent mean flux having a maximum value at the intermediate plasma region, followed by a continuous decrease with radius, eventually tending to zero at the outer radial locations, where the plasma column is extremely rarefied. The experimental setup in W7-AS consists of a reciprocating Langmuir probe moving from the scrape-off-layer inwards, allowing to characterize radial turbulent fluxes around that plasma locations.

The scarcity of experimental entries, and hence, of avalanche events, has led to perform the statistical analysis of avalanche events in terms of survival functions instead of the more common probability distribution functions. A criteria based on amplitude thresholding for the determination of avalanche events has been chosen throughout all the work. Furthermore, maximum/minimum thresholds are set based on the first n maxima/minima of the input signal ($n = 10$).

The amount of total avalanche events in SLPM is roughly uniform with radius except at the outermost radial locations where an increasing trend is observed. A higher amount of positive (outwards) avalanches is found at the innermost ($r < 1.3$ cm) and outermost ($r > 2.5$ cm) radial locations. Conversely, a higher amount of negative (inwards) avalanches is found at the intermediate (1.3 cm $< r <$ 2.5 cm) radial locations. Since the overall net radial turbulent flux is consistently positive at all radial positions, it is inferred that in the intermediate radial region, outward events are, on average, of higher intensity (i.e., size) than inward events.

The distributions of avalanche sizes, avalanche durations and inter-avalanche quiet-times in SLPM exhibit general exponential behaviour within the relevant space-time ranges associated to the mesoscale, pointing to trivial, diffusive transport dynamics, in the inner and middle radial area ($r < 2.6$ cm) of the plasma column. Nevertheless, at the outermost radial location ($r \geq 2.6$ cm), the tails of avalanche sizes/durations and inter-avalanche quiet-times distributions present power-law trends, pointing to a departure from diffusion.

The size-duration scaling relation in SLPM at the outermost radial location, $\gamma_{ST}(r = 2.8) \simeq 1.2$, is in line with findings through size/duration/quiet-time avalanche distributions. The set of exponents match well with the fundamental scaling relation given by Eq. (9), found in distinct physical and biological processes.

Results coming from radial turbulent fluxes just inside the LCMS in the W7-AS stellarator resemble those found at the outer region of SLPM. The dynamics behaves as would be expected if a more kind of complex, non-diffusive processes would indeed dominate transport.

The diffusive character of plasma transport found in a significant portion of the radial range ($r < 2.6$ cm) of the plasma column in SLPM, is consistent with past theoretical studies in the context of diffusive sandpiles[14, 15, 16] and numerical simulations of drift-wave turbulence[17, 18]. In those works, it was shown that the coexistence of an intermittent turbulent transport channel associated to near-marginal dynamics, which is inherent in many fusion plasmas, together with any additional (subdominant) diffusive transport channel (such as, for instance, classical or neoclassical transport or supermarginal turbulence) could prevent the establishment of long-term correlations even when the intensity of the second channel is very low relative to the intensity of the first. The explanation was that long-term memory effects are the consequence of local inhomogeneities stored in the (density/temperature/pressure) profiles, but in the presence of a second transport channel such as Coulomb collisions, which basically smooths out any inhomogeneity in the profiles, long-term memory effects are completely erased. It is not clear the importance of Coulomb collisions in SLPM since, on one hand, the low degree of ionization ($\sim 10\%$) suggests that their influence on transport, if any, should be irrelevant, but on the other hand, the low temperatures (a few electronvolts) could make plasma collisions important to a certain extent. In any case, it seems that is just enough to impede the establishment of long-term memory effects. Alternatively, axial losses due to the free streaming of particles along the open magnetic field lines could be another memory-erasing mechanism.

Non-diffusive features develop in SLPM as we probe the outermost radial region ($r > 2.6$ cm) of the plasma column. A possible explanation accounting for this dynamical transition can be found in the fact that the electron temperature profile shows a huge gradient at radial interval $r > 2.5$ cm, being quite uniform at radial interval $r < 2.5$ cm[19]. A reasonable hypothesis in view of the extended power laws is that a kind of electron temperature gradient instability is dominating radial transport at the edge[31].

It is important to emphasize the need for a proper methodology when dealing with avalanche statistics. First, appropriate amplitude and duration thresholdings are demanded in order to separate the gaussian noise from real avalanches. Secondly, the use of survival functions (or cumulative distribution functions) instead of the more common pdfs can be helpful in determining the presence of gaussian/self-similar features (i.e., exponential/power-law distributions tails).

It is perhaps also worthwhile to mention here that the kind of non-diffusive transport discussed in this paper is rather different in nature to that associated to blob transport in the scrape-off layer of tokamaks. Blob cross-field transport is also known to be non-diffusive, but it has an almost ballistic character attributed to the $\mathbf{E} \times \mathbf{B}$ drift resulting from the charge separation that takes place within the blob, not needing any extended spatial correlations. We would also say that we have not tried to look into the role played by zonal flows, that may play an important role in reducing radial/temporal correlations whenever their associated scales allow it, due to the fact that we cannot estimate them from the available data.

Finally, all experimental results presented in this paper have been obtained via Eulerian measurements (i.e., through Langmuir probes located at specific spatial locations). This constitutes a severe restriction for the determination of possible long-range spatial structures, specifically for the determination of avalanches. A way to improve all the work done in this article is to perform measurements using several (at least two) probes spatially separated (either in the radial, poloidal or even in the axial direction), to analyze spatial correlations and thus determine more appropriately the spatial structure of the avalanches studied here.

Acknowledgments

This research has been sponsored by Spanish Ministerio de Ciencia e Innovación, Projects No. PID2019-110734RB-I00 and No. PID2022-137869OB-I00.

References

[1] B. B. Kadomtsev, "Plasma Turbulence," Academic Press, London, 1965.

[2] N. A. Krall and A. W. Trivelpiece, "Principles of Plasma Physics," McGraw Hill, New York, 1973.

[3] C. C. Petty, T. C. Luce, K. H. Burrell, S. C. Chiu, J. S. deGrassie, C. B. Forest, P. Gohil, C. M. Greenfield, R. J. Groebner, R. W. Harvey, R. I. Pinsker, R. Prater and R. E. Waltz, "Nondimensional transport scaling in DIII-D: Bohm versus gyro-Bohm resolved," Phys. Plasmas **2**, 2342 (1995).

[4] P. H. Diamond and T. S. Hahm, "On the dynamics of turbulent transport near marginal stability," Phys. Plasmas **2**, 3640 (1995).

[5] B. A. Carreras, V. E. Lynch and B. LaBombard, "Structure and properties of the electrostatic fluctuations in the far scrape-off layer region of Alcator C-Mod," Phys. Plasmas **8**, 3702 (2001).

[6] R. Sánchez, B. Ph. van Milligen and B. A. Carreras, "Probabilistic transport models for plasma transport in the presence of critical thresholds: Beyond the diffusive paradigm," Phys. Plasmas **12**, 056105 (2005).

[7] D. R. Demers, P. M. Schoch, T. P. Crowley, K. A. Connor and A. Ouroua, "Radial electrostatic flux inferred from core measurements of potential and density fluctuations," Phys. Plasmas **8**, 1278 (2001).

[8] L. G. Eliseev *et al*, "Evaluation of Turbulent Particle Flux by Heavy Ion Beam Probe in the T-10 Tokamak," Plasma and Fusion Research **13**, 3402106 (2018).

[9] A. V. Melnikov *et al*, "Alfvén eigenmode properties and dynamics in the TJ-II stellarator," Nucl. Fusion **52**, 123004 (2012).

[10] C. Riccardi, D. Xuantong, M. Salierno, L. Gamberale and M. Fontanesi, "Experimental analysis of drift waves destabilization in a toroidal plasma," Phys. Plasmas **4**, 3749 (1997).

[11] G. Y. Antar, S. I. Krasheninnikov, P. Devynck, R. P. Doerner, E. M. Hollmann, J. A. Boedo, S. C. Luckhardt and R. W. Conn, "Experimental Evidence of Intermittent Convection

in the Edge of Magnetic Confinement Devices," Phys. Rev. Lett. **87**, 065001 (2001).

[12] V. P. Budaev, S. Takamura, N. Ohno and S. Masuzaki, "Superdiffusion and multifractal statistics of edge plasma turbulence in fusion devices," Nucl. Fusion **46**, S181-S191 (2006).

[13] J. A. Mier, R. Sanchez, D. E. Newman, O. F. Castellanos, E. Anabitarte, J. M. Senties and B. Ph. van Milligen, "Characterization of radial turbulent fluxes in the Santander linear plasma machine," Phys. Plasmas **21**, 052303 (2014).

[14] D. E. Newman, B. A. Carreras, P. H. Diamond and T. S. Hahm, "The dynamics of marginality and self-organized criticality as a paradigm for turbulent transport," Phys. Plasmas **3**, 1858 (1996).

[15] R. Sanchez, D. E. Newman and B. A. Carreras, "Mixed SOC diffusive dynamics as a paradigm for transport in fusion devices," Nucl. Fusion **41**, 247 (2001).

[16] J. A. Mier, R. Sánchez and D. E. Newman, "Tracer particle transport dynamics in the diffusive sandpile cellular automaton," Chaos, Solitons and Fractals **140**, 110117 (2020).

[17] J. A. Mier, L. García and R. Sánchez, "Study of the interaction between diffusive and avalanche-like transport in near-critical dissipative-trapped-electron-mode turbulence," Phys. Plasmas **13**, 112308 (2006).

[18] J. A. Mier, R. Sánchez, L. García, D. E. Newman and B. E. Carreras, "On the nature of transport in near-critical dissipative-trapped-electron-mode turbulence: Effect of a subdominant diffusive channel," Phys. Plasmas **15**, 112301 (2008).

[19] O. F. Castellanos, E. Anabitarte, J. M. Senties, C. Hidalgo and M. A. Pedrosa, "Parallel flows and turbulence in a linear plasma machine," Plasma Phys. Controlled Fusion **47**, 2067 (2005).

[20] H. Renner *et al*, "Initial operation of the wendelstein 7AS advanced stellarator," Plasma Phys. Controlled Fusion **31**, 1579 (1989).

[21] M. Hirsch *et al*, "Major results from the stellarator Wendelstein 7-AS," Plasma Phys. Controlled Fusion **50**, 053001 (2008).

[22] F. Wagner *et al*, "W7-AS: One step of the Wendelstein stellarator line," Phys. Plasmas **12**, 072509 (2005).

[23] R. Sánchez, B. Ph. van Milligen, D. E. Newman and B. A. Carreras, "Quiet-Time Statistics of Electrostatic Turbulent Fluxes from the JET Tokamak and the W7-AS and TJ-II Stellarators," Phys. Rev. Lett. **90**, 185005 (2003).

[24] R. Sánchez and D. E. Newman, "Self-organized criticality and the dynamics of near-marginal turbulent transport in magnetically confined fusion plasmas," Plasma Phys. Controlled Fusion **57**, 123002 (2015).

[25] K. Ida, "Non-local transport nature revealed by the research in transient phenomena of toroidal plasma," Rev. Mod. Plasma Phys. **6**, 2 (2022).

[26] G. L. Ragan, "Microwave Transmission Circuits," MIT Radiation Laboratory Series 9, McGraw Hill, New York (1950).

[27] M. Endler, H. Niedermeyer, L. Giannone, E. Holzhauer, A. Rudyj, G. Theimer, N. Tsois and the ASDEX Team, "Measurements and modelling of electrostatic fluctuations in the scrape-off layer of ASDEX," Nucl. Fusion **35**, 1307 (1995).

[28] H. Lin, Roger D. Bengtson and Ch. P. Ritz, "Temperature fluctuations and transport in a tokamak adge plasma," Phys. Fluids B **1**, 2027 (1989).

[29] C. Hidalgo, R. Balbin, M. A. Pedrosa, I. Garcia-Cortes and M. A. Ochando, "Experimental evidence of significant temperature fluctuations in the plasma edge region of the TJ-I tokamak," Phys. Rev. Lett. **69**, 1205 (1992).

[30] E. Spada, V. Carbone, R. Cavazzana, L. Fattorini, G. Regnoli, N. Vianello, V. Antoni, E. Martines, G. Serianni, M. Spolaore and L. Tramontin, "Search of Self-Organized Criticality Processes in Magnetically Confined Plasmas: Hints from the Reversed Field Pinch Configuration," Phys. Rev. Lett. **86**, 3032 (2001).

[31] O. F. Castellanos, J. M. López, J. M. Sentíes and E. Anabitarte, "Intermittency, avalanche statistics, and long-term correlations in a turbulent plasma," J. Stat. Mech. **2013**, P04022.

[32] R. Sanchez and D. E. Newman, "A primer on complex systems," Springer-Verlag, Heidelberg (2018).

[33] T. Hwa and M. Kardar, "Avalanches, hydrodynamics, and discharge events in models of sandpiles," Phys. Rev. A **45**, 7002 (1992).

[34] J. A. Mier, R. Sanchez and D. E. Newman, "Characterization of a transition in the transport dynamics of a diffusive sandpile by means of recurrence quantification analysis," Phys. Rev. E **94**, 022128 (2016).

[35] D. R. Cox and V. Isham, "Point processes," Chapman & Hall, 1980.

[36] J. P. Klein and M. L. Moeschberger, "Statistics for Biology and Health", Springer-Verlag, New York, 1997.

[37] G. Boffeta, V. Carbone, P. Giuliani, P. Veltri and A. Vulpiani, "Power Laws in Solar Flares: Self-Organized Criticality or Turbulence?," Phys. Rev. Lett. **83**, 4662 (1999).

[38] S. Papanikolaou, F. Bohn, R. L. Sommer, G. Durin, S. Zapperi and P. Sethna, "Universality beyond power laws and the average avalanche shape," Nature Phys. **7**, 316 (2011).

[39] R. Sánchez, D. E. Newman, W. Ferenbaugh, B. A. Carreras, V. E. Lynch and B. Ph. van Milligen, "Quiet-time statistics: A tool to probe the dynamics of self-organized-criticality systems from within the strong overlapping regime," Phys. Rev. E **66**, 036124 (2002).

[40] J. P. Sethna, K. A. Dahmen and C. R. Myers, "Crackling noise," Nature **410**, 242 (2001).

[41] N. Friedman, S. Ito, B. A. Brikman, M. Shimono, R. E. Lee DeVille, K. A. Dahmen, J. M. Beggs and T. C. Butler, "Universal Critical Dynamics in High Resolution Neuronal Avalanche Data," Phys. Rev. Lett. **108**, 208102 (2012).

[42] J. M. Beggs and D. Plenz, "Neuronal Avalanches in Neocortical Circuits," J. Neurosci. **23**, 11167 (2003).

[43] F. Lombardi, H. J. Herrmann, C. Perrone-Capano, D. Plenz and L. de Arcangelis, "Balance between Excitation and Inhibition Controls the Temporal Organization of Neuronal Avalanches," Phys. Rev. Lett. **108**, 228703 (2012).